RESEARCH ARTICLE

Targeted renal knockdown of Na^+/H^+ exchanger regulatory factor *Sip1* produces uric acid nephrolithiasis in *Drosophila*

Saurav Ghimire[1], Selim Terhzaz[1], Pablo Cabrero[1], Michael F. Romero[2], Shireen A. Davies[1] and Julian A. T. Dow[1]*

[1] Institute of Molecular, Cell & Systems Biology, College of Medical, Veterinary & Life Sciences, University of Glasgow, Glasgow G12 8QQ, United Kingdom

[2] Department of Physiology and Biomedical Engineering, Mayo Clinic College of Medicine & Science, Rochester, Minnesota 55905, United States of America

Running head: Sip1 and urate nephrolithiasis

Correspondence:

Prof. Julian A.T. Dow

Institute of Molecular, Cell & Systems Biology, College of Medical, Veterinary & Life Sciences, University of Glasgow, Glasgow G12 8QQ, United Kingdom

Email: Julian.Dow@glasgow.ac.uk

Abstract

Nephrolithiasis is one of the most common kidney diseases, with poorly understood pathophysiology, but experimental study has been hindered by lack of experimentally tractable models. *Drosophila melanogaster* is a useful model organism for renal diseases because of genetic and functional similarities of Malpighian (renal) tubules with the human kidney. Here, we demonstrate the function of *Sip1* (SRY-interacting protein 1) gene, an orthologue of human *NHERF*1, in *Drosophila* MTs, and its impact on nephrolithiasis. Abundant birefringent calculi were observed in *Sip1* mutant flies, and the phenotype was also observed in renal stellate cell-specific RNAi *Sip1* knockdowns in otherwise normal flies, confirming a renal aetiology. This phenotype was abolished in *rosy* mutant flies (which model human xanthinuria) and by the xanthine oxidase inhibitor allopurinol, suggesting that the calculi were of uric acid. This was confirmed by direct biochemical assay for urate. Stones rapidly dissolved when the tubule was bathed in alkaline media, suggesting that *Sip1* knockdown was acidifying the tubule. SIP1 was shown to co-locate with Na^+/H^+ exchanger NHE2, and with Moesin, in stellate cells. Knockdown of *NHE2* specifically to the stellate cells also increased renal uric acid stone formation and so a model was developed in which SIP1 normally regulates NHE2 activity and luminal pH, ultimately leading to uric acid stone formation. *Drosophila* renal tubule may thus offer a useful model for urate nephrolithiasis.

Keywords: *Drosophila*, Nephrolithiasis, Malpighian Tubules, *Sip1*, Uric acid stones

Introduction

Nephrolithiasis is a common renal disease, with a high and increasing prevalence rate (5% in women and 12% in men) (13), but with poorly understood aetiology. Despite a large amount of investment in treatment, research and medication of the disease worldwide (>US$ 5.3 billion/year in the US alone) (31), limited progress in the medical treatment of nephrolithiasis has been achieved in the last few decades (54) (40). The incidence of nephrolithiasis has been increasing in parallel with other epidemics such as cardiovascular disease and hypertension (21), depression (28), diabetes mellitus (71) and metabolic diseases (54). For example, the prevalence rate of uric acid is increasing globally, i.e. in the US by > 1%, in N. Europe between 0.4% to 0.7% and in S. Europe by > 3% (60).

Although all the underlying causes behind the formation of kidney stones are not fully known, the literature suggests genetics as a crucial factor in susceptibility to some types of nephrolithiasis (4, 18) along with environmental and dietary factors (40, 43). There are two main models describing the role of genetics in kidney stone formation; the monogenic co-dominant model (26), in which a single gene actively accelerates stone accumulation (24), and the polygenic or heterogeneous co-inheritance model (52, 63) in which two or more genes act coherently to each other to accelerate or inhibit stone accumulation (25, 51). Thus, basic research to determine the role of genes in stone formation with new animal models to investigate the pathophysiology of the disease may play a vital role in the advancement of the field, leading to new therapeutic agents for the management of the kidney disease (36).

Approximately 70% of *D. melanogaster* genes have human homologs, many of which are associated with kidney diseases (18). With its transparent renal system and powerful genetic technologies, *Drosophila* is an ideal system to study several different types of nephrolithiasis (2, 3, 10, 12, 18, 30, 40, 61, 72, 73). The *Drosophila* renal system comprises two pairs of Malpighian tubules (MTs); one anterior and one posterior (68) with critical roles in excretion and osmoregulation, functionally analogous to mammalian kidneys. MTs are composed of two major cell types, principal cells (PCs) and stellate cells (SCs), which are responsible for ion, water and organic solute transport (5, 17, 40). MTs regulate body calcium, magnesium, potassium, phosphate and carbonate levels, thereby influencing the formation of intraluminal stones (18).

Here, we demonstrate a novel role of the *SRY interacting protein 1* (*Sip1* or *CG10939*) gene, an ortholog of human Na^{+}/H^{+} exchanger regulatory factor (*NHERF1*) (32), in renal uric acid stone formation by selective knockdown of *Sip1* in stellate cells. To identify the intraluminally accumulated stones, we performed physiological, chemical pharmacological and genetic analyses including the development of a chemical approach to quantify uric acid accumulation in MTs. *Sip1*, *Moesin and NHE2* were co-localised in wild-type, *Sip1* mutant, and *Moesin* RNAi flies, suggesting a model in which *Sip1* regulates *NHE2* to regulate luminal H^{+}, resulting in a favourable environment for uric acid stone formation.

Materials and Methods

Drosophila stocks

D. melanogaster strains were reared at 22°C, 55% humidity in 12:12 h light: dark photoperiod on standard cornmeal diet. The following strains were used: Canton-S (CS) as wild-type, UAS-*CG10939* RNAi (BDSC, #65156), UAS-*Moe* RNAi (BDSC, #31135), and the *rosy*^{1} *(ry*^{1}*)* mutant (BDSC, #584) (42) were obtained from the Bloomington stock centre (Bloomington, IN, USA), *UAS-NHE2 RNAi* (VDRC

#106053) from Vienna Drosophila Research centre (Vienna, Austria). UAS-DRIP-eYFP was described in (8). UAS lines were driven by either *CapaR-Gal4* - specific to tubule principal cells (59), or *ClC-a-Gal4* - specific to tubule stellate cells (8). The mutant *Sip1*^{5a}*/CyO* (49) line was a kind gift from Dr Cédric Polesello (Toulouse, France). Fly crosses were performed at 26°C to increase the efficiency of the GAL4/UAS binary system.

Dietary allopurinol assay

Allopurinol [4-hydroxypyrazolo (3,4-d) pyrimidine; Sigma] was dissolved in standard *Drosophila* diet to make final concentration 250 ng/ml (75) and kept in vials at room temperature for one day. 5-7 days old adult flies were transferred in the drug-containing vials and kept for two days before dissection and imaging steps. The following lines were fed with allopurinol: Wild-type (WT), *Sip1*$^{(-/-)}$ and *ry*$^{(-/-)}$.

RNA preparation and qRT-PCR

Knockdown efficiency of the targeted gene relative to parental lines was assessed by quantitative RT-PCR (qRT-PCR). Tubules were dissected from 50 flies of specified genotype and RNA was isolated using RNeasy® Mini Kit (Qiagen) following manufacturers recommendations. cDNA was generated using the protocol as described elsewhere (7). qRT-PCR was performed using an Opticon DNA engine 4 (Bio-Rad Technologies) using Brilliant III Ultra-Fast SYBR Green QPCR master mix (Agilent) using the primer sequences, *Sip1* (*CG10939*) F, GCTGTTCGCTTTCGTTTCGTTTAG, R, TGTCCTGGTTTCACCTTCTCCG; *NHE2* (*CG9256*) F, CACAATGTCCTGGCTGACCTTTC, R, CTCCACCACCGAGAGATAAAACC, *Rpl32* (*CG7939*), F, TGACCATCCGCCCAGCATAC, R, ATCTCGCCGCAGTAAACGC. The specificity of amplicons was verified with melting curve analysis, and the messenger level was normalised using *Rpl32* as an internal control gene, and expression level was calculated using the ΔΔCt method (37).

Imaging and pH sensitivity of renal stones

Adult flies (5-7 days old) were dissected in Phosphate Buffered Saline (PBS, pH 5), and intact MTs were mounted on glass-slide in PBS adjusted to pH 5 to 10, and the MTs were immediately imaged using a microscope (Axioskop 2, Zeiss) under polarised light. As the visualisation of the birefringent crystals is transitory, intact tubule samples, from wild-type and from specified genotypes, were imaged immediately after dissection. Images were taken every minute for 30 min and were quantified once the time frame was completed. Imaging conditions were maintained as described previously (11). Total stones present within the tubule at 0 min were considered 100% and the stones accumulated after 1, 10, 20 and 30 min were quantified with respect to the initial quantity.

Quantification of renal stones

Quantification of the stones was achieved by using Image J software as per the protocol described previously (11). Briefly, the tubular area of interest was outlined, and the pixel intensity was obtained. Any tubular pixel intensity above the threshold was considered stones. The total area of stones in the lumen was calculated by subtracting background intensity.

Immunohistochemistry

Immunostaining procedures were performed as described previously (8). Adult MTs were dissected in PBS and fixed with 4% (w/v) paraformaldehyde for 30 min at room temperature. The following primary antibodies were used: rabbit anti-NHE2 (short isoform), (1:300); rabbit anti-NHE2 (long isoform), (1:300) (15); rabbit anti-MOE-P and rabbit anti-SIP1, (1:200) (53). Alexa Fluor 488/546 goat-anti-rabbit (Thermo Fisher Scientific) was used in a dilution of 1:1000 for visualisation of the primary antiserum. Incubations in the primary and secondary antibodies were performed overnight. Tubules were incubated with markers such as 4',6-diamidino-2-phenylindole (DAPI; Sigma-Aldrich, 1 µg/ml) and/or Rhodamine-Alexa-633-coupled phalloidin (Thermo Fisher Scientific, 1:100). All samples were mounted in Vectashield (Vector Laboratories), and images were taken using a confocal microscope (LSM 800 Zeiss) and processed with Zen software and Adobe Photoshop/Illustrator CS 5.1.

Uric acid colorimetric assay

Total quantity of uric acid stones accumulated in whole tubules homogenates of wild-type, *Sip1* mutant and *Sip1/NHE2* knockdown flies was quantified using the Quantichrome Colorimetric Uric acid kit (DIUA-250, BioAssay Systems) according to the manufacturer's instruction. Six adult fly MTs per sample were homogenised in 12 µl of Tween-20 (Sigma-Aldrich), and 200 µl of working reagent was added to 5 µl of each tubule sample in 96 well plates (3 replicates for each sample). Samples were incubated for 30 minutes at room temperature and the optical density measured at 590nm using a Mithras LB940 automated 96-well plate reader (Berthold Technologies). Data were analysed using the MikroWin software.

Statistical analysis

Data are presented as mean ± SEM. The significance of differences was assessed with Student's *t*-test (two-tailed) for unpaired samples or one-way ANOVA followed by Dunnett's test, with significance taken as $p<0.05$, marked graphically with an asterisk.

Results

Mutation of *Sip1* induces stones accumulation

Mammalian studies have shown that NHERF1 may play an important role in renal stone formation(35), so we determined the role of the *Drosophila* orthologue *NHERF1, Sip1,* in mediating stone formation in *Drosophila* MTs. Immunocytochemical study using anti-SIP1 showed that SIP1 was indeed expressed in wild-type fly kidney, but specifically in the SCs which are easily recognisable by their stellar shape (Figure 1 A). No immunostaining was detected in the MTs of homozygous *Sip1* mutants (Figure 1 A), thus confirming that the signal observed in wild-type corresponds to SIP1 protein, and that SIP1 expression is abolished in the *Sip1* homozygous mutants.

We next investigated the stone phenotype of the MTs of *Sip1* mutant flies. Mutation of *Sip1* results in the formation of a very high number of small birefringent stones in the lumen of both male and female MTs compared to wild-type tubules (Figure 1 B-G). Quantification of the mineralised area covered between 70-80% of both anterior and posterior tubule area of male and female flies (Figure 1 H and I). The anterior tubules have an enlarged initial segment (58, 69), which handles most of the organism's excess calcium (20); however, this region did not develop birefringent stones in *Sip1* mutants, and the stone burden was similar in anterior and posterior tubules (Figure 1), suggesting that these calculi were not calcium-based.

We next investigated whether renal, cell-specific knockdown of *Sip1* resulted in the same phenotype. The *UAS-Sip1RNAi* line produced a significant knockdown (>70%) in overall tubule expression of *Sip1* when driven in SCs (*ClC-a-Gal4>UAS-Sip1 RNAi*) (Figure 2 A). Specific silencing of *Sip1* gene in SCs showed marked increase of birefringent stones compared to parental control lines (*ClC-a-Gal4/+, UAS-Sip1 RNAi/+*) (Figure 2 B and C). However, no knockdown was observed when *Sip1* RNAi was driven in PCs (Figure 2 D), suggesting that *Sip1* is expressed uniquely in the SCs. Accordingly, specific knockdown of *Sip1* gene in tubule PCs using *CapaR-Gal4* driver line resulted in unchanged stone quantity compared to controls (Figure 2 E), indicating a novel role of *Sip1* in tubule SCs in mediating stone formation. Taken together, these results suggest that mutation of *Sip1,* and specific knockdown of *Sip1* in SCs, promotes lithiasis.

Modulation of pH affects stone solubility

To determine the chemical nature of the intraluminally accumulated stones, *Sip1* mutant tubules were incubated under acid or alkaline load by altering bathing pH between 5 and 10. At pH 5 and pH 6, no change in the quantity of stones after 30 minutes was noted. However, at pH 7, the total accumulated stones started to dissolve significantly within 20 mins, and this process occurred faster with increased pH of the bathing solution, where 90% of the stones were dissolved within 10 min at pH 10 (Figure 3 A).

To precisely determine at which pH stones start dissolving, the pH of the bathing solution was altered by 0.1 pH unit ranging between pH 6 and pH 7. We showed that intraluminal stones start dissolving significantly at pH 6.7 and above (Figure 3 B and C). Uric acid is a weak acid (pKa 5.5 (38, 55)), that is relatively insoluble compared with its sodium salt (33, 70). Therefore, the stones accumulated in *Sip1* mutant MTs share similar chemical behaviour with uric acid stones.

Inhibition of the function of Xanthine Oxidase leads to the disappearance of the stones in *Sip1* mutant tubules

Uric acid is a product of purine metabolism (Figure 4 A). The pathway includes Xanthine Oxidase (XO) which is responsible for converting hypoxanthine to xanthine; and xanthine to uric acid. Allopurinol inhibits the function of XO, thereby blocking the biosynthesis of uric acid (48) and a concomitant increase of hypoxanthine and xanthine concentration (47). *Rosy* (*ry*) is the second mutation discovered in *Drosophila melanogaster* (18), and encodes the enzyme xanthine dehydrogenase/xanthine oxidase. *Rosy* mutant closely recapitulate the symptoms of human xanthinuria type I (16, 65). In particular, both *ry* mutants and allopurinol-treated flies show elevated hypoxanthine and xanthine, and extremely low levels of urate and allantoin, as shown by metabolomic analysis (1, 34). Therefore, we studied the formation of calculi in both *Sip1* and *rosy* mutants under feeding treatment with allopurinol. In standard diet, wild-type and *rosy* flies (with no XO enzyme activity) do not produce uric acid stones (Figure 4 B, D and F). Furthermore, wild-type, *Sip1* and *rosy* mutants were fed allopurinol-containing diet, leading to the disappearance of birefringent crystals in the MTs (Figure 4 C, E and G), phenocopying the xanthine stone (*ry* flies) (Figure 4 F). Thus, pharmacological inhibition of XO by dietary exposure of allopurinol led to the disappearance of stones, confirming that the intraluminally accumulated stones are uric acid stones.

Uric acid quantification in *Sip1* knockdown tubules

We next quantified the concentration of the uric acid in the MTs of wild-type, *Sip1* mutant and SCs specific *Sip1* knockdown flies. The total concentration of uric acid in the MTs of *Sip1* mutant flies was 8.5-fold higher compared to wild-type flies (Figure 5

A). Similarly, in lines in which *Sip1* RNAi is targeted to MT SCs (*ClC-a-Gal4>UAS-Sip1 RNAi*), a 3-fold increase in the quantity of uric acid compared to the parental controls was observed (*ClC-a-Gal4/+* and *UAS-Sip1 RNAi/+*) (Figure 5 B).

Taken altogether, these results unambiguously demonstrate the presence of uric acid stones within MTs of *Sip1* mutant and *Sip1* knockdown flies, and that *Sip1* gene expression in the SCs mediates proper tubular lumen acidification.

***Sip1* and *Moesin* localise to the apical membrane of tubule SCs**

Sip1 encodes a protein that functions as a scaffold linking the plasma membrane and cytoskeletal linker proteins encoded by *Moesin* (32), where SIP1 and Moesin interact with each other to maintain epithelial integrity via phosphorylation (32, 50). We tested the co-localisation of these proteins in MTs using polyclonal antibodies raised against both SIP1 and Moesin. SIP1 immunostaining was detected exclusively in the SCs of *ClC-a-Gal4>UAS-DRIP-Venus* MTs expressing DRIP-eYFP, a marker of apical membranes in SCs (Figure 6 A). An optical section made through one of the SCs clearly emphasize that SIP1 and DRIP-eYFP colocalised to the luminal side of nucleus (Figure 6 B-D).

Moesin is known to participate with Crumbs in development of apical basal polarity, and to mark the apical domain of epithelia (39, 41) . Immunostaining using anti-Moesin also showed specific labelling of Moesin only in SCs (Figure 6 E), and a z-stack image revealed that the subcellular location was on the apical side of the plasma membrane (Figure 6 F). As expected, no immunostaining was observed in tubules from *Moesin* knockdown flies (Figure 6 G and H), confirming the specificity of the antibody. These results confirm that SIP1 and Moesin are both localised to the apical membrane in polarized epithelial SCs which suggest potential functional relationship.

SIP1 colocalizes with Na^+/H^+ Exchanger NHE2 and Moesin in SCs

The function of NHEs was first characterised in isolated cortical brush-border membrane vesicles showing Na^+-driven H^+ movement and H^+-driven Na^+ movement across the membrane (44). Further, computational modelling of the hydrophobic-hydrophilic nature and predicted structure of NHEs has also shown interaction between NHEs with NHERF1/SIP1 (46). It is known that SIP1 is a scaffold protein required for the regulation of several transmembrane receptors and ion transporters (32, 62), so we hypothesised that SIP1 could regulate the activity of alkali-metal/proton exchanger (NHE) protein family in *Drosophila* tubules.

NHEs play an important role in the transport of Na^+ and H^+ across the membrane (22) as well maintenance of the cellular and epithelial integrity. *D. melanogaster* has three *NHE* genes - *NHE1*, *NHE2*, and *NHE3*, which are expressed in multiple tissues (Supplementary Figure 1) (22), but NHE2 long isoform is stellate cell-specific (Figure 8) (15). Interestingly, we found that *NHE2-long* isoform also has clear localisation in SCs of wild-type MTs; whilst *NHE2-short* antibody labels the apical membrane of tubule PCs (Supplementary Figure 2). Further, when Moesin was specifically knocked down in MT SCs, no birefringent crystals were observed in *Moesin* RNAi lines (*ClC-a-Gal4>UAS-Moesin RNAi*) (data not shown) compared to parental controls (*ClC-a-Gal4/*+ and *UAS-Moesin RNAi/*+) suggesting the absence of the role of Moesin alone in the formation of uric acid stones. However, specific knockdown of *NHE2* in SCs (~70%) resulted in higher intraluminal accumulation of birefringent stones (~30% of the tubule area (Figure 7 A), and the solubilised uric acid levels quantified using the colorimetric assay were significantly increased compared to parental lines (**Error! Reference source not found.**Figure 7 B-D). Interestingly, no such phenotype was observed in PCs specific *NHE2* knockdown (Figure 7 E). Taken together, these results demonstrate the roles of *Sip1* and *NHE2* in renal urate nephrolithiasis.

Consistent with the co-localisation of SIP1*,* *Moesin* and *NHE*2 proteins, we investigated a putative functional relationship between these proteins. To achieve this, we used an immunocytochemistry approach using anti-NHE2 long and anti-NHE2 short rabbit polyclonal antibodies to stain tubules of *Sip1* and *Moesin* mutant flies. Interestingly, no immunostaining using both NHE antibodies was observed in tubules from *Sip1* and *Moesin* mutant flies, suggesting that SIP1, Moesin and NHE proteins are part of a scaffold linking the plasma membrane and cytoskeleton of tubule stellate cells (Figure 8 and Supplementary Figure 2).

Discussion

Mammalian NHERF1 was first characterised in rabbit border membrane as an essential cofactor for cyclic AMP inhibition of Na^+/H^+ exchanger (45, 66). Here, the role of the *Drosophila* orthologue *NHERF1, Sip1,* in mediating uric acid stone formation in *Drosophila* MTs. was characterised by biochemical, pharmacological and genetic assays. Insects, like birds, are considered to have uricotelic excretory systems, in which waste nitrogen is dumped as uric acid, in order to conserve water, and so uric acid calculi are constitutive in most terrestrial insects (19). However, adult *Drosophila* tubules express very high levels of urate oxidase (uricase) (64), and so urate crystals are not normally abundant. In this context, the extreme accumulations observed here in *Sip1* mutants are remarkable.

What mediates precipitation of uric acid stones in the tubule? In mammals, interaction between SIP1 and urate transporters has been suggested (14); our results suggest SIP1 connects plasma membrane proteins such as NHE2, with members of the ERM (Ezrin, Radixin, Moesin) family, thereby regulating lumen acidification (32, 62). In mammals, ERM protein complex interacts with the plasma membrane and actin cytoskeleton (29, 67) within specific domains to systematise the plasma membrane (27) and thereby providing a regulated linkage between the plasma membrane and the actin cytoskeleton. Recent genetic and biochemical studies have shown that *NHERF1/Sip1* plays an essential role in the activation of ERM proteins in mammals (6) and also in *D. melanogaster* (32). Intriguingly, targeted deletion of *NHERF1* in mouse elevates intestinal deposition of calcium and also triggers calcium oxalate and uric acid crystal formation (57). However, loss of ERM proteins results in mislocalization of NHERF1 in mouse (56). In *D. melanogaster, Moesin* is the sole representative of the ERM family (53). *Sip1* promotes *Moesin* function by affecting interaction with *Slik Kinase*; genetic and functional interactions between *Sip1*, *Moesin* and *Slik kinase* has been shown in *Drosophila* pupae and cultured S2 cells (32). We demonstrated expression of SIP1 and Moesin in the MT SCs, potentially suggesting an interaction in SCs.

Na^+/H^+ exchangers (NHEs) are integral membrane proteins which comprises multiple transmembrane domains and a large cytosolic carboxyl-terminal domain (74). Studies in the mammalian model have shown that NHERF1 phosphorylates NHEs thereby affecting their activity (9). Interestingly, rabbit NHERF1 is involved in the regulation of the renal brush border NHEs (23). Also, computational modelling of the hydrophobic-hydrophilic nature and predicted structure of NHEs has also shown the interaction between NHEs with NHERF1 (46). In support with these previous findings, our immunocytochemistry experiments reveal that NHE2 (long) is localised to MT SCs but are not expressed in *Sip1* and *Moesin* mutant MTs. Thus, all three proteins; SIP1, Moesin, and NHEs are localised specifically in stellate cells with potential functional interactions.

Collectively, our experimental results allow a model for the formation of uric acid stones in the MTs of *D. melanogaster* (Figure 9). Although our model does not allow us to distinguish uric acid stones from hyperuricosuria alone (rare), aciduria (very common) or both, we demonstrate that a common class of kidney stones can usefully be studied in the *Drosophila* renal system, where it can benefit from the uniquely powerful genetic interventions characteristic of this organism.

Acknowledgements

We are grateful to Dr Cédric Polesello, Toulouse University, for providing *Drosophila* fly strains and reagents and to Dr Guillermo Martinez Corrales for his experimental assistance. This work was supported by the European Union's Horizon 2020 research and innovation programme under Marie Skłodowska-Curie Grant agreement N^{o}64293 RENALTRACT to JATD and SD, by the UK Biotechnology and Biological Sciences Research Council (BBSRC) grant BB/L002647/1 (SD, JATD and ST) and NIH grants R01-DK092408 and U54-DK100227 (JATD, MFR).

References

1. **Al Bratty M, Hobani Y, Dow JAT, and Watson DG.** Metabolomic profiling of the effects of allopurinol on *Drosophila melanogaster*. *Metabolomics* DOI 10.1007/s11306-011-0275-6, 2011.
2. **Ali SN, Dayarathna TK, Ali AN, Osumah T, Ahmed M, Cooper TT, Power NE, Zhang D, Kim D, Kim R, St Amant A, Hou J, Tailly T, Yang J, Luyt L, Spagnuolo PA, Burton JP, Razvi H, and Leong HS.** Drosophila melanogaster as a function-based high-throughput screening model for anti-nephrolithiasis agents in kidney stone patients. *Dis Model Mech*, 2018.

3. **Assimos D.** Re: Ethylene glycol induces calcium oxalate crystal deposition in malpighian tubules: a Drosophila model for nephrolithiasis/urolithiasis. *J Urol* 187: 1299-1300, 2012.
4. **Bagga HS, Chi T, Miller J, and Stoller ML.** New insights into the pathogenesis of renal calculi. *Urologic Clinics of North America* 40: 1-12, 2013.
5. **Beyenbach KW, Skaer H, and Dow JAT.** The developmental, molecular, and transport biology of Malpighian tubules. *Annual Review of Entomology* 55: 351-374, 2010.
6. **Brône B and Eggermont J.** PDZ proteins retain and regulate membrane transporters in polarized epithelial cell membranes. *American Journal of Physiology-Cell Physiology* 288: C20-C29, 2005.
7. **Cabrero P, Radford JC, Broderick KE, Costes L, Veenstra JA, Spana EP, Davies SA, and Dow JA.** The Dh gene of Drosophila melanogaster encodes a diuretic peptide that acts through cyclic AMP. *Journal of Experimental Biology* 205: 3799-3807, 2002.
8. **Cabrero P, Terhzaz S, Romero MF, Davies SA, Blumenthal EM, and Dow JA.** Chloride channels in stellate cells are essential for uniquely high secretion rates in neuropeptide-stimulated Drosophila diuresis. *Proceedings of the National Academy of Sciences* 111: 14301-14306, 2014.
9. **Centonze M, Saponaro C, and Mangia A.** NHERF1 Between Promises and Hopes: Overview on Cancer and Prospective Openings. *Translational oncology* 11: 374-390, 2018.
10. **Chen YH, Liu HP, Chen HY, Tsai FJ, Chang CH, Lee YJ, Lin WY, and Chen WC.** Ethylene glycol induces calcium oxalate crystal deposition in Malpighian tubules: a Drosophila model for nephrolithiasis/urolithiasis. *Kidney Int* 80: 369-377, 2011.
11. **Chi T, Kim MS, Lang S, Bose N, Kahn A, Flechner L, Blaschko SD, Zee T, Muteliefu G, and Bond N.** A Drosophila model identifies a critical role for zinc in mineralization for kidney stone disease. *PloS one* 10: e0124150, 2015.
12. **Chung VY and Turney BW.** A Drosophila genetic model of nephrolithiasis: transcriptional changes in response to diet induced stone formation. *BMC Urol* 17: 109, 2017.
13. **Coe FL, Evan A, and Worcester E.** Kidney stone disease. *The Journal of clinical investigation* 115: 2598-2608, 2005.
14. **Cunningham R, Brazie M, Kanumuru S, Xiaofei E, Biswas R, Wang F, Steplock D, Wade JB, Anzai N, and Endou H.** Sodium-hydrogen exchanger regulatory factor-1 interacts with mouse urate transporter 1 to regulate renal proximal tubule uric acid transport. *Journal of the American Society of Nephrology* 18: 1419-1425, 2007.
15. **Day JP, Wan S, Allan AK, Kean L, Davies SA, Gray JV, and Dow JA.** Identification of two partners from the bacterial Kef exchanger family for the apical plasma membrane V-ATPase of Metazoa. *Journal of cell science* 121: 2612-2619, 2008.
16. **Dent CE and Philpot GR.** Xanthinuria: an inborn error of metabolism. *Lancet* I: 182-185, 1954.
17. **Dow JA and Davies SA.** The Drosophila melanogaster malpighian tubule. *Advances in Insect Physiology* 28: 1-83, 2001.
18. **Dow JA and Romero MF.** Drosophila provides rapid modeling of renal development, function, and disease. *American Journal of Physiology-Renal Physiology* 299: F1237-F1244, 2010.
19. **Dow JAT.** Excretion and salt and water regulation. In: *The insects: structure & function / R.F. Chapman*, edited by Simpson SJ and Douglas AE. Cambridge, UK: Cambridge University Press, 2012, p. 546-587.
20. **Dube K, McDonald DG, and O'Donnell MJ.** Calcium transport by isolated anterior and posterior Malpighian tubules of Drosophila melanogaster: roles of sequestration and secretion. *J Insect Physiol* 46: 1449-1460, 2000.
21. **Fuster V and Kelly BB.** Epidemiology of cardiovascular disease. 2010.
22. **Giannakou ME and Dow JA.** Characterization of the Drosophila melanogaster alkali-metal/proton exchanger (NHE) gene family. *Journal of Experimental Biology* 204: 3703-3716, 2001.
23. **Giral H, Cranston D, Lanzano L, Caldas Y, Sutherland E, Rachelson J, Dobrinskikh E, Weinman EJ, Doctor RB, and Gratton E.** NHE3 regulatory factor 1 (NHERF1) modulates intestinal

sodium-dependent phosphate transporter (NaPi-2b) expression in apical microvilli. *Journal of Biological Chemistry* 287: 35047-35056, 2012.

24. **Goldfarb DS.** The search for monogenic causes of kidney stones: Am Soc Nephrol, 2014.

25. **Griffin D.** A review of the heritability of idiopathic nephrolithiasis. *Journal of clinical pathology* 57: 793-796, 2004.

26. **Halbritter J, Baum M, Hynes AM, Rice SJ, Thwaites DT, Gucev ZS, Fisher B, Spaneas L, Porath JD, and Braun DA.** Fourteen monogenic genes account for 15% of nephrolithiasis/nephrocalcinosis. *Journal of the American Society of Nephrology*: ASN. 2014040388, 2014.

27. **Hanzel D, Reggio H, Bretscher A, Forte J, and Mangeat P.** The secretion-stimulated 80K phosphoprotein of parietal cells is ezrin, and has properties of a membrane cytoskeletal linker in the induced apical microvilli. *The EMBO Journal* 10: 2363, 1991.

28. **Hidaka BH.** Depression as a disease of modernity: explanations for increasing prevalence. *Journal of affective disorders* 140: 205-214, 2012.

29. **Hirao M, Sato N, Kondo T, Yonemura S, Monden M, Sasaki T, Takai Y, and Tsukita S.** Regulation mechanism of ERM (ezrin/radixin/moesin) protein/plasma membrane association: possible involvement of phosphatidylinositol turnover and Rho-dependent signaling pathway. *The Journal of cell biology* 135: 37-51, 1996.

30. **Hirata T, Cabrero P, Berholtz DS, Bondeson DP, Ritman EL, Thompson JR, Dow JA, and Romero MF.** *In vivo Drosophila* genetic model for calcium oxalate nephrolithiasis. *Am J Physiol Renal Physiol* 303: F1555-1562, 2012.

31. **Hirata T, Cabrero P, Berkholz DS, Bondeson DP, Ritman EL, Thompson JR, Dow JA, and Romero MF.** In vivo Drosophilia genetic model for calcium oxalate nephrolithiasis. *American Journal of Physiology-Renal Physiology* 303: F1555-F1562, 2012.

32. **Hughes SC, Formstecher E, and Fehon RG.** Sip1, the Drosophila orthologue of EBP50/NHERF1, functions with the sterile 20 family kinase Slik to regulate Moesin activity. *J Cell Sci* 123: 1099-1107, 2010.

33. **Iwata H, Nishio S, Yokoyama M, Matsumoto A, and Takeuchi M.** Solubility of uric acid and supersaturation of monosodium urate: why is uric acid so highly soluble in urine? *J Urol* 142: 1095-1098, 1989.

34. **Kamleh MA, Hobani Y, Dow JAT, and Watson DG.** Metabolomic profiling of *Drosophila* using liquid chromatography Fourier transform mass spectrometry. *FEBS Lett* 582: 2916-2922, 2008.

35. **Karim Z, Gerard B, Bakouh N, Alili R, Leroy C, Beck L, Silve C, Planelles G, Urena-Torres P, Grandchamp B, Friedlander G, and Prie D.** NHERF1 mutations and responsiveness of renal parathyroid hormone. *N Engl J Med* 359: 1128-1135, 2008.

36. **Knauf F and Preisig PA.** Drosophila: a fruitful model for calcium oxalate nephrolithiasis&quest. *Kidney international* 80: 327-329, 2011.

37. **Livak KJ and Schmittgen TD.** Analysis of relative gene expression data using real-time quantitative PCR and the 2− ΔΔCT method. *methods* 25: 402-408, 2001.

38. **Martillo MA, Nazzal L, and Crittenden DB.** The crystallization of monosodium urate. *Current rheumatology reports* 16: 400, 2014.

39. **Medina E, Williams J, Klipfell E, Zarnescu D, Thomas G, and Le Bivic A.** Crumbs interacts with moesin and beta(Heavy)-spectrin in the apical membrane skeleton of Drosophila. *J Cell Biol* 158: 941-951, 2002.

40. **Miller J, Chi T, Kapahi P, Kahn AJ, Kim MS, Hirata T, Romero MF, Dow JA, and Stoller ML.** Drosophila melanogaster as an emerging translational model of human nephrolithiasis. *The Journal of urology* 190: 1648-1656, 2013.

41. **Miller KG.** A role for moesin in polarity. *Trends Cell Biol* 13: 165-168, 2003.

42. **Mitchell HK and Glassman E.** Hypoxanthine in rosy and maroon-like mutants of Drosophila melanogaster. *Science* 129: 268, 1959.

43. **Moe OW.** Kidney stones: pathophysiology and medical management. *The Lancet* 367: 333-344, 2006.

44. **Murer H, Hopfer U, and Kinne R.** Sodium/proton antiport in brush-border-membrane vesicles isolated from rat small intestine and kidney. 1976. *Journal of the American Society of Nephrology* 9: 143-150, 1998.

45. **Murtazina R, Kovbasnjuk O, Zachos NC, Li X, Chen Y, Hubbard A, Hogema BM, Steplock D, Seidler U, and Hoque KM.** Tissue-specific regulation of sodium/proton exchanger isoform 3 activity in Na+/H+ exchanger regulatory factor 1 (NHERF1) null mice cAMP inhibition is differentially dependent on NHERF1 and exchange protein directly activated by cAMP in ileum versus proximal tubule. *Journal of Biological Chemistry* 282: 25141-25151, 2007.

46. **Orlowski J and Grinstein S.** Diversity of the mammalian sodium/proton exchanger SLC9 gene family. *Pflügers Archiv* 447: 549-565, 2004.

47. **Pacher P, Nivorozhkin A, and Szabó C.** Therapeutic effects of xanthine oxidase inhibitors: renaissance half a century after the discovery of allopurinol. *Pharmacological reviews* 58: 87-114, 2006.

48. **Parks DA and Granger DN.** Xanthine oxidase: biochemistry, distribution and physiology. *Acta physiologica Scandinavica Supplementum* 548: 87, 1986.

49. **Polesello C, Delon I, Valenti P, Ferrer P, and Payre F.** Dmoesin controls actin-based cell shape and polarity during Drosophila melanogaster oogenesis. *Nature cell biology* 4: 782-789, 2002.

50. **Ponuwei GA.** A glimpse of the ERM proteins. *Journal of biomedical science* 23: 35, 2016.

51. **Ranabir S, Baruah MP, and Devi KR.** Nephrolithiasis: endocrine evaluation. *Indian journal of endocrinology and metabolism* 16: 228, 2012.

52. **Resnick M, Pridgen DB, and Goodman HO.** Genetic predisposition to formation of calcium oxalate renal calculi. *New England Journal of Medicine* 278: 1313-1318, 1968.

53. **Roch F, Polesello C, Roubinet C, Martin M, Roy C, Valenti P, Carreno S, Mangeat P, and Payre F.** Differential roles of PtdIns (4, 5) P2 and phosphorylation in moesin activation during Drosophila development. *J Cell Sci* 123: 2058-2067, 2010.

54. **Romero V, Akpinar H, and Assimos DG.** Kidney stones: a global picture of prevalence, incidence, and associated risk factors. *Reviews in urology* 12: e86, 2010.

55. **Sakhaee K and Maalouf NM.** Metabolic syndrome and uric acid nephrolithiasis. *Seminars in nephrology*. Elsevier, 2008, p. 174-180.

56. **Saotome I, Curto M, and McClatchey AI.** Ezrin is essential for epithelial organization and villus morphogenesis in the developing intestine. *Developmental cell* 6: 855-864, 2004.

57. **Shenolikar S.** Targeted disruption of the mouse gene encoding a PDZ domain containing protein adaptor, NHERF-1, promotes Npt2 internalization and renal phosphate wasting. *Proc Natl Acad Sci USA* 99: 11470-11475, 2002.

58. **Sözen MA, Armstrong JD, Yang MY, Kaiser K, and Dow JAT.** Functional domains are specified to single-cell resolution in a *Drosophila* epithelium. *Proceedings of the National Academy of Sciences of the United States of America* 94: 5207-5212, 1997.

59. **Terhzaz S, Cabrero P, Robben JH, Radford JC, Hudson BD, Milligan G, Dow JA, and Davies S-A.** Mechanism and function of Drosophila capa GPCR: a desiccation stress-responsive receptor with functional homology to human neuromedinU receptor. *PloS one* 7: e29897, 2012.

60. **Trinchieri A and Montanari E.** Prevalence of renal uric acid stones in the adult. *Urolithiasis* 45: 553-562, 2017.

61. **Tzou DT, Taguchi K, Chi T, and Stoller ML.** Animal models of urinary stone disease. *International Journal of Surgery*, 2016.

62. **Vaquero J, Ho-Bouldoires TN, Clapéron A, and Fouassier L.** Role of the PDZ-scaffold protein NHERF1/EBP50 in cancer biology: from signaling regulation to clinical relevance. *Oncogene* 36: 3067, 2017.

63. **Vezzoli G, Soldati L, and Gambaro G.** Update on primary hypercalciuria from a genetic perspective. *The Journal of urology* 179: 1676-1682, 2008.

64. **Wallrath LL, Burnett JB, and Friedman TB.** Molecular characterization of the *Drosophila melanogaster* urate oxidase gene, an ecdysone-repressible gene expressed only in the Malpighian tubules. *Mol Cell Biol* 10: 5114-5127, 1990.

65. **Wang J, Kean L, Yang J, Allan AK, Davies SA, Herzyk P, and Dow JAT.** Function-informed transcriptome analysis of *Drosophila* renal tubule. *Genome Biology* 5: R69, 2004.

66. **Weinman EJ, Dubinsky W, and Shenolikar S.** Regulation of the renal Na+-H+ exchanger by protein phosphorylation. *Kidney international* 36: 519-525, 1989.

67. **Weinman EJ, Steplock D, Wang Y, and Shenolikar S.** Characterization of a protein cofactor that mediates protein kinase A regulation of the renal brush border membrane Na (+)-H+ exchanger. *Journal of Clinical Investigation* 95: 2143, 1995.

68. **Wessing A and Eichelberg D.** Malpighian tubules, rectal papillae and excretion. *Genetics and biology of Drosophila*, 1979.

69. **Wessing A and Eichelberg D.** Malpighian tubules, rectal papillae and excretion. In: *The genetics and biology of Drosophila*, edited by Ashburner A and Wright TRF. London: Academic Press, 1978, p. 1-42.

70. **Wilcox WR, Khalaf A, Weinberger A, Kippen I, and Klinenberg JR.** Solubility of uric acid and monosodium urate. *Med Biol Eng* 10: 522-531, 1972.

71. **Wild S, Roglic G, Green A, Sicree R, and King H.** Global prevalence of diabetes: estimates for the year 2000 and projections for 2030. *Diabetes care* 27: 1047-1053, 2004.

72. **Wu SY, Shen JL, Man KM, Lee YJ, Chen HY, Chen YH, Tsai KS, Tsai FJ, Lin WY, and Chen WC.** An emerging translational model to screen potential medicinal plants for nephrolithiasis, an independent risk factor for chronic kidney disease. *Evid Based Complement Alternat Med* 2014: 972958, 2014.

73. **Yang H, Male M, Li Y, Wang N, Zhao C, Jin S, Hu J, Chen Z, Ye Z, and Xu H.** Efficacy of Hydroxy-L-proline (HYP) analogs in the treatment of primary hyperoxaluria in Drosophila Melanogaster. *BMC Nephrol* 19: 167, 2018.

74. **Yoshida M, Zhao L, Grigoryan G, Shim H, He P, and Yun CC.** Deletion of Na+/H+ exchanger regulatory factor 2 represses colon cancer progress by suppression of Stat3 and CD24. *American Journal of Physiology-Gastrointestinal and Liver Physiology* 310: G586-G598, 2016.

75. **Zhou X and Riddiford LM.** rosy function is required for juvenile hormone effects in Drosophila melanogaster. *Genetics* 178: 273-281, 2008.

Figure legends

Figure 1. Mutation of *Sip1* causes accumulation of stones intraluminally. (A) SIP1 protein is specifically expressed in MT SCs of wild-type (WT) fly, while no expression was detected in *Sip1* mutant flies. DAPI (blue), SIP1 (green), scale bars: 10 µm. (B-G) Representative polarised microscopy images of WT and *Sip1*$^{(-/-)}$ mutant flies, immediately after dissection (at time 0). *Sip1*$^{(-/-)}$ MTs show intraluminal accumulation of birefringent stones. Bars represent the percentage of total stones in the anterior and posterior MTs of male (H) and female (I). *Sip1* mutant flies compared to wild-type MTs. Bar diagrams were constructed by considering the accumulated stones at time 0 as 100%. Data are presented as mean ± SEM, N=5. Where *p<0.05, one-way ANOVA followed by Dunnett's test. In panels B-G, scale bars: 500 µm.

Figure 2. Quantification of stones accumulated in the lumen of *Sip1* knockdown MTs. (A) The expression of *Sip1* was significantly decreased in *Clc-a-Gal4>UAS-Sip1* MTs as compared to parental lines, *ClC-a-Gal4/+* and *UAS-Sip1 RNAi/+*. (B) Representative polarised microscopy images of *Clc-a-Gal4>UAS-Sip1* RNAi knockdown flies compared to parental controls. (C) Quantification of stones accumulated in the MTs of knockdown (SCs specific) and control conditions. (D) The expression of *Sip1* shows no downregulation when specifically knockdown in PCs. (E) Representative polarised images of MTs of PCs *Sip1* knockdown flies (*CapaR-Gal4>UAS-Sip1 RNAi*) as compared to parental lines, *CapaR-Gal4/+* and *UAS-Sip1 RNAi/+*. Data are presented as mean ± SEM, N=5, *p<0.05, one way ANOVA followed by Dunnet's test. In panels B and E, scale bars: 500 µm.

Figure 3. pH modulates solubility of MT stones. (A) The graph represents the percentage of undissolved stones corresponding to the pH change of the bathing solution. (B-C) Bar diagram represents the pH (pH 6.6 and 6.7) at which stones start dissolving over a 30 min period. Data are expressed as mean ± SEM, N=5. *p<0.05, which One-way ANOVA followed by Dunnett's test, NS stands for non-significant.

Figure 4. Biochemical pathway for uric acid formation and blockade by allopurinol. (A) Uric acid biosynthesis pathway. Uric acid is the end product of purine metabolism catalysed by different enzymes, including Xanthine Oxidase. (B-G) Representative images of MTs from *Sip1* and *ry* mutants in normal or allopurinol diet. In all cases, flies fed with allopurinol did not accumulate stones. In panels B-G, scale bars: 500 µm.

Figure 5. Concentration of uric acid in *Sip1* mutant and knockdown flies. (A) Solubilized levels of uric acid in *Sip1* mutant MTs are significantly higher compared to control tubules. (B) Uric acid concentration is significantly higher in MTs of *Sip1*

knockdown flies (*Clc-a-Gal4>UAS-Sip1* RNAi) compared to parental lines. Data are presented as mean ± SEM, N=5. *p<0.05, Student's *t*-test (A), one way ANOVA followed by Dunnett's test (B).

Figure 6. SIP1 protein is expressed in the apical membrane of SCs. (A) Immunostaining of adult MTs using anti-SIP1 antibody in *ClC-a-Gal4>UAS-DRIP-Venus* expressing DRIP-eYFP, a marker of apical membranes in stellate cells. (B-D) Cross section of a single SC showing colocalization between SIP1 and DRIP-eYFP in the apical membrane. (E) Expression of Moesin protein in MT SCs. (F) Moesin is specifically expressed in the apical membrane of the MT SCs of wild-type flies while no expression was seen in *Moesin* knockdown (KD) flies respectively (G-H). DAPI (blue), SIP1 (red), Moesin (green), Scale bars: (A and E): 100 µm, (B-D and F-H): 10 µm.

Figure 7. Silencing of *NHE2* in SCs of MTs causes accumulation of stones. (A) The expression of *NHE2* was significantly decreased in knockdown flies *ClC-a-Gal4>UAS-NHE2 RNAi* compared to parental controls *ClC-a-Gal4/+* and *UAS-NHE2 RNAi/+*. (B) Representative polarized microscopic images of *NHE2* knockdown flies and parental controls. Scale bars: 500 µm. (C) Quantification of the stones accumulated in *NHE2* knockdown MTs. (D-E) Quantification of the uric acid concentration accumulated in SCs and PCs specific *NHE2* knockdown MTs. Data are presented as mean ± SEM, N=5. *p<0.05, one-way ANOVA followed by Dunnett's test. NS stands for non-significant.

Figure 8. Expression of NHE2-long in wild-type, *Sip1* mutant and *Moesin* knockdown flies. NHE2-long isoform shows clear localization in the apical membrane of MT SCs. Thin bright lines represent nonspecific staining of trachea, which are known to be sticky to antibodies. DAPI (blue), NHE2-short (green). Scale bars: 20 µm.

Figure 9. Model illustrating the role of SIP1 protein in uric acid stone formation in *Drosophila* Malpighian tubules. MTs contain two main cell types, principal (grey) and stellate (yellow) cells and the transport processes cell are described elsewhere (5) . In principal cells, the apically localized V-type H^+ ATPase energizes transepithelial secretion, providing electrogenic transport of H^+ into the lumen, coupled with a cation/H^+ antiporter. In stellate cells, chloride ions move down an electrochemical gradient through chloride channels in SCs and water follows by osmosis through water channels in SCs (Cabrero *et al.*, 2019, in prep.). The apically located SIP1 interacts with NHE2 and activates the efflux Na^+ and influx of H^+. Mutation of *Sip1* and *NHE2* lead to accumulation of H^+ ions intraluminally and tubular lumen acidification, mediating uric acid stone formation.

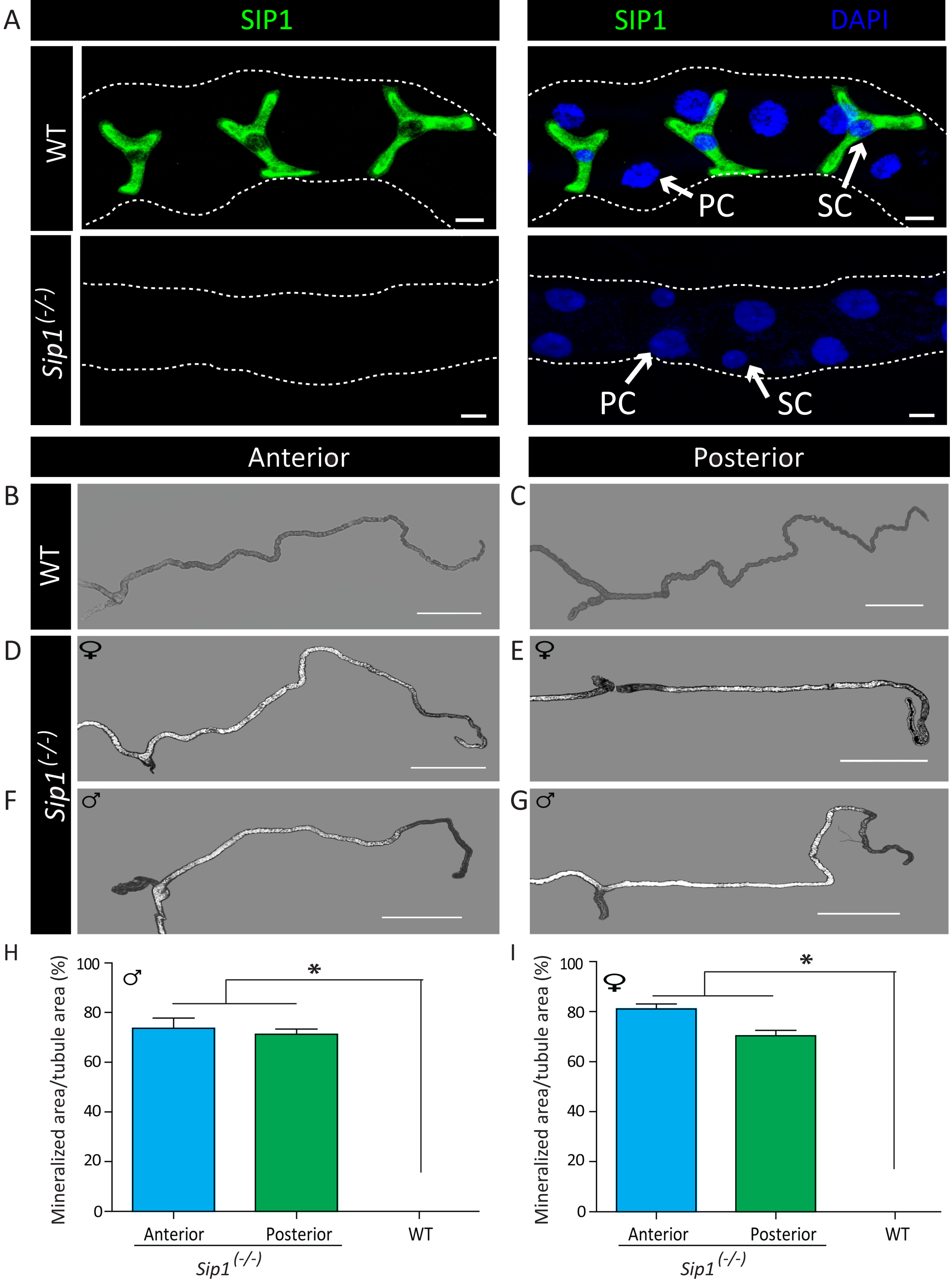
A
SIP1
SIP1
DAPI
WT
PC
SC
Sip1 (-/-)
PC
SC
Anterior
Posterior
B
C
WT
D
♀
E
♀
Sip1 (-/-)
F
♂
G
♂
H
Mineralized area/tubule area (%)
100
80
60
40
20
0
♂
*
Anterior
Posterior
WT
Sip1 (-/-)
I
Mineralized area/tubule area (%)
100
80
60
40
20
0
♀
*
Anterior
Posterior
WT
Sip1 (-/-)

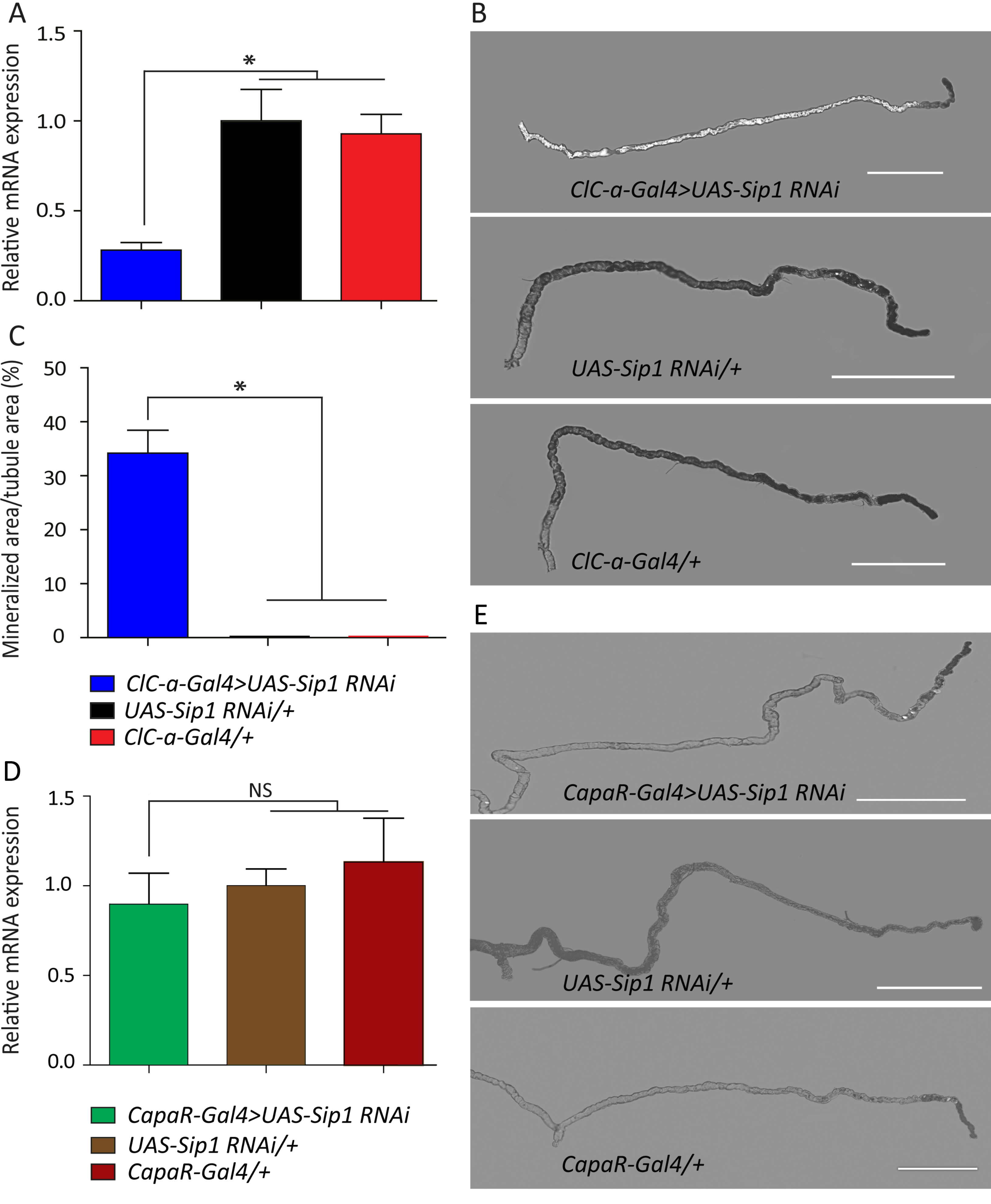

A
1.5
1.0
0.5
0.0
Relative mRNA expression
*
B
ClC-a-Gal4>UAS-Sip1 RNAi
UAS-Sip1 RNAi/+
ClC-a-Gal4/+
C
50
40
30
20
10
0
Mineralized area/tubule area (%)
*
ClC-a-Gal4>UAS-Sip1 RNAi
UAS-Sip1 RNAi/+
ClC-a-Gal4/+
D
1.5
1.0
0.5
0.0
Relative mRNA expression
NS
CapaR-Gal4>UAS-Sip1 RNAi
UAS-Sip1 RNAi/+
CapaR-Gal4/+
E
CapaR-Gal4>UAS-Sip1 RNAi
UAS-Sip1 RNAi/+
CapaR-Gal4/+

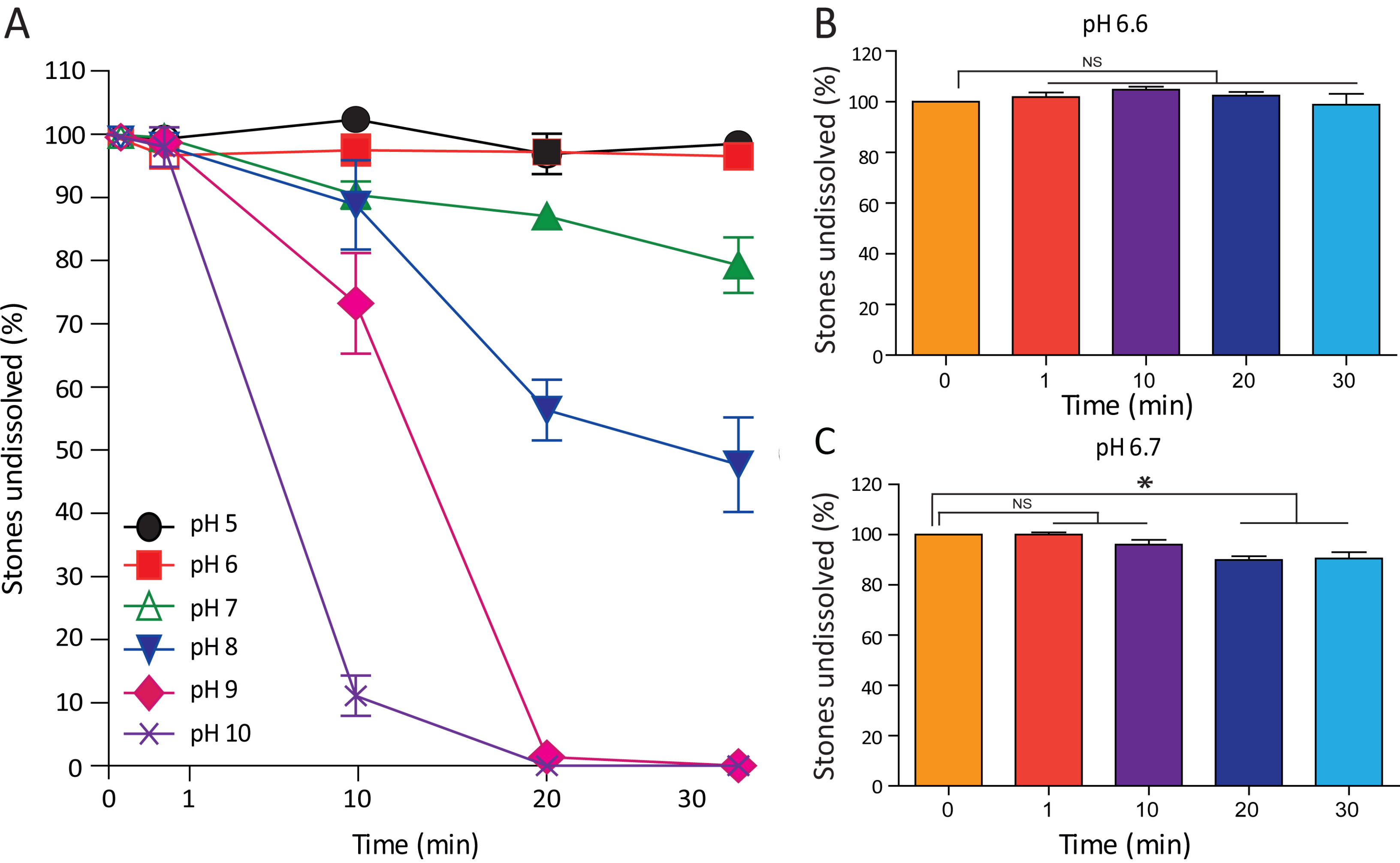
A
110
100
90
80
70
60
50
40
30
20
10
0
Stones undissolved (%)
0
1
10
20
30
Time (min)
pH 5
pH 6
pH 7
pH 8
pH 9
pH 10
B
pH 6.6
NS
120
100
80
60
40
20
0
Stones undissolved (%)
0
1
10
20
30
Time (min)
C
pH 6.7
*
NS
120
100
80
60
40
20
0
Stones undissolved (%)
0
1
10
20
30
Time (min)

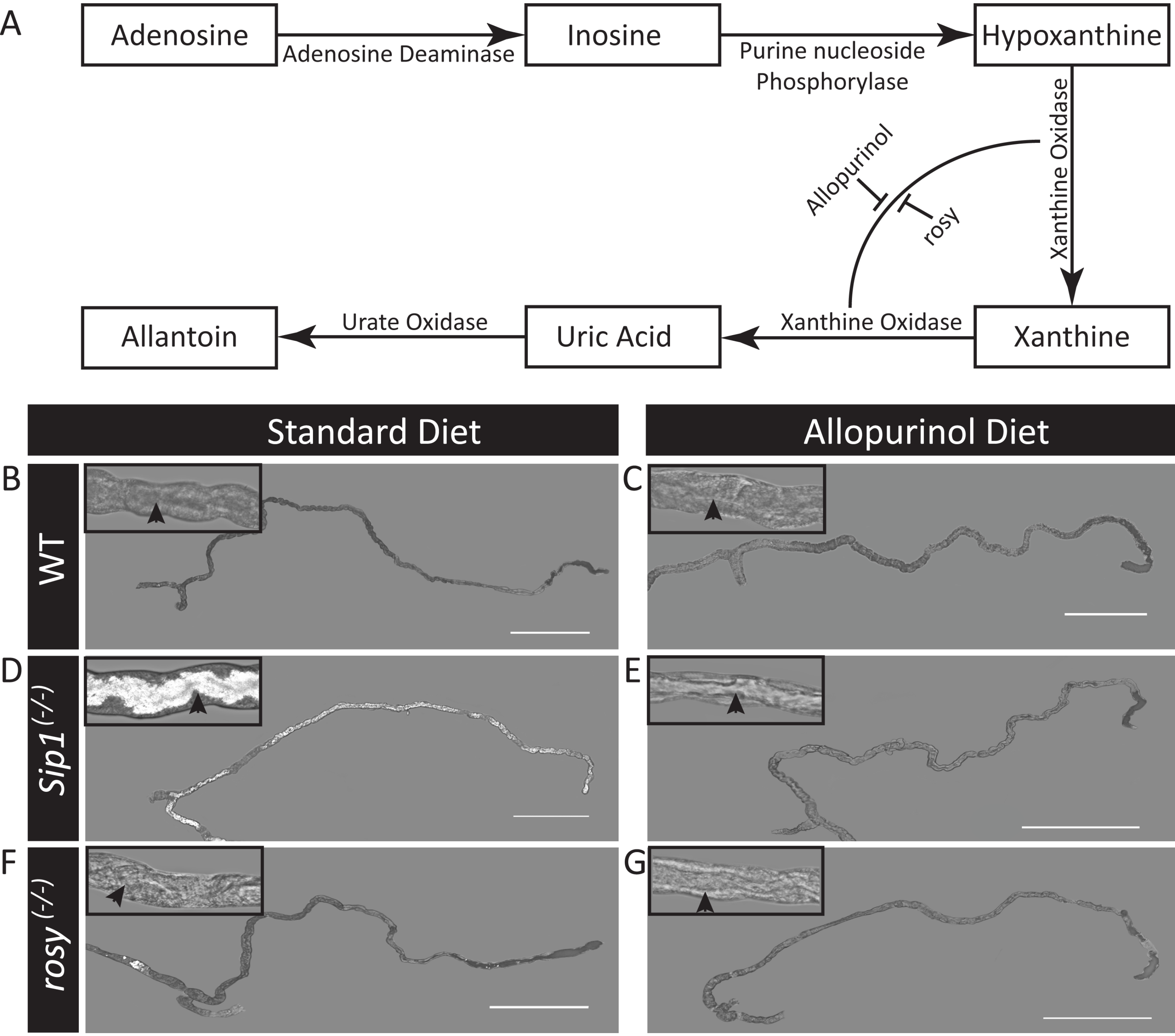
A
Adenosine
Adenosine Deaminase
Inosine
Purine nucleoside
Phosphorylase
Hypoxanthine
Xanthine Oxidase
Allopurinol
rosy
Xanthine
Xanthine Oxidase
Uric Acid
Urate Oxidase
Allantoin
Standard Diet
Allopurinol Diet
B
C
WT
D
E
Sip1(-/-)
F
G
rosy(-/-)

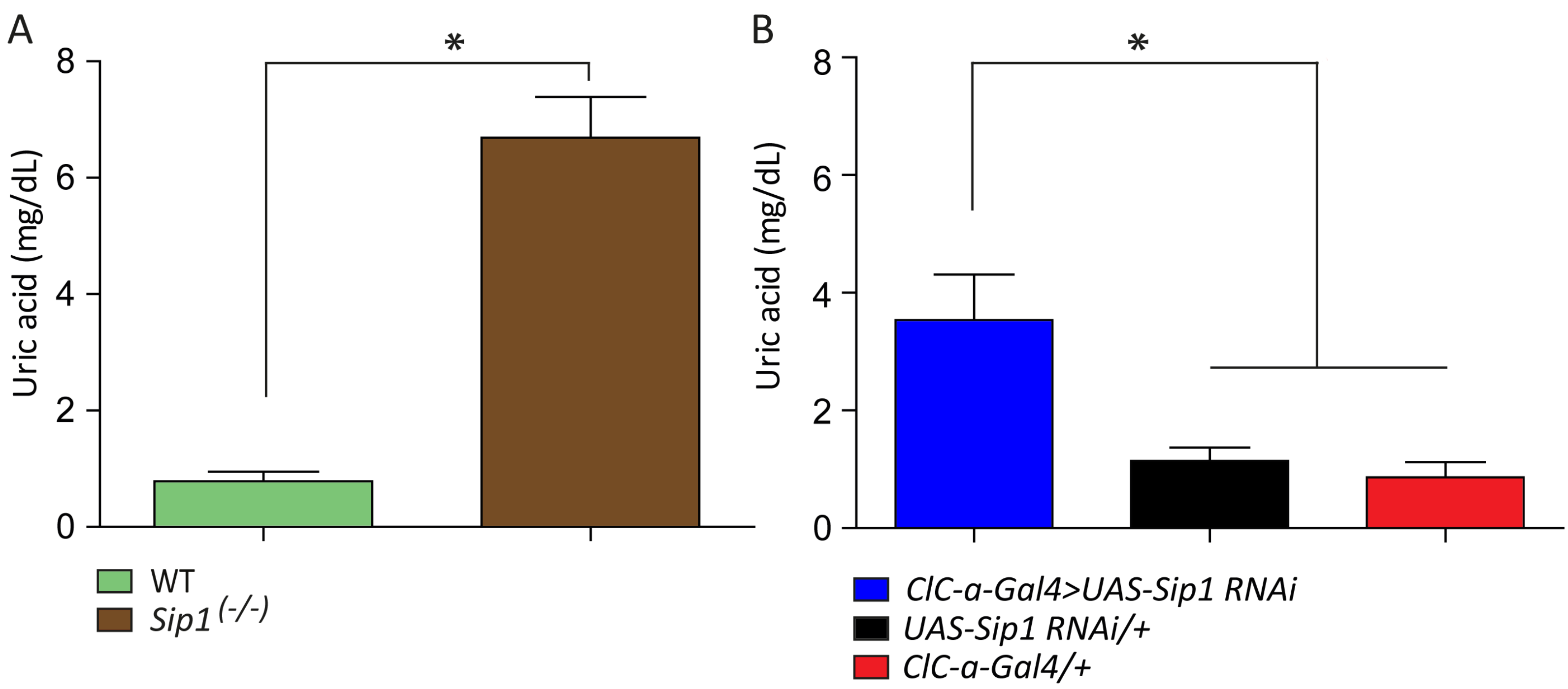

A
B
*
*
Uric acid (mg/dL)
Uric acid (mg/dL)
0
2
4
6
8
WT
Sip1 (-/-)
ClC-a-Gal4>UAS-Sip1 RNAi
UAS-Sip1 RNAi/+
ClC-a-Gal4/+

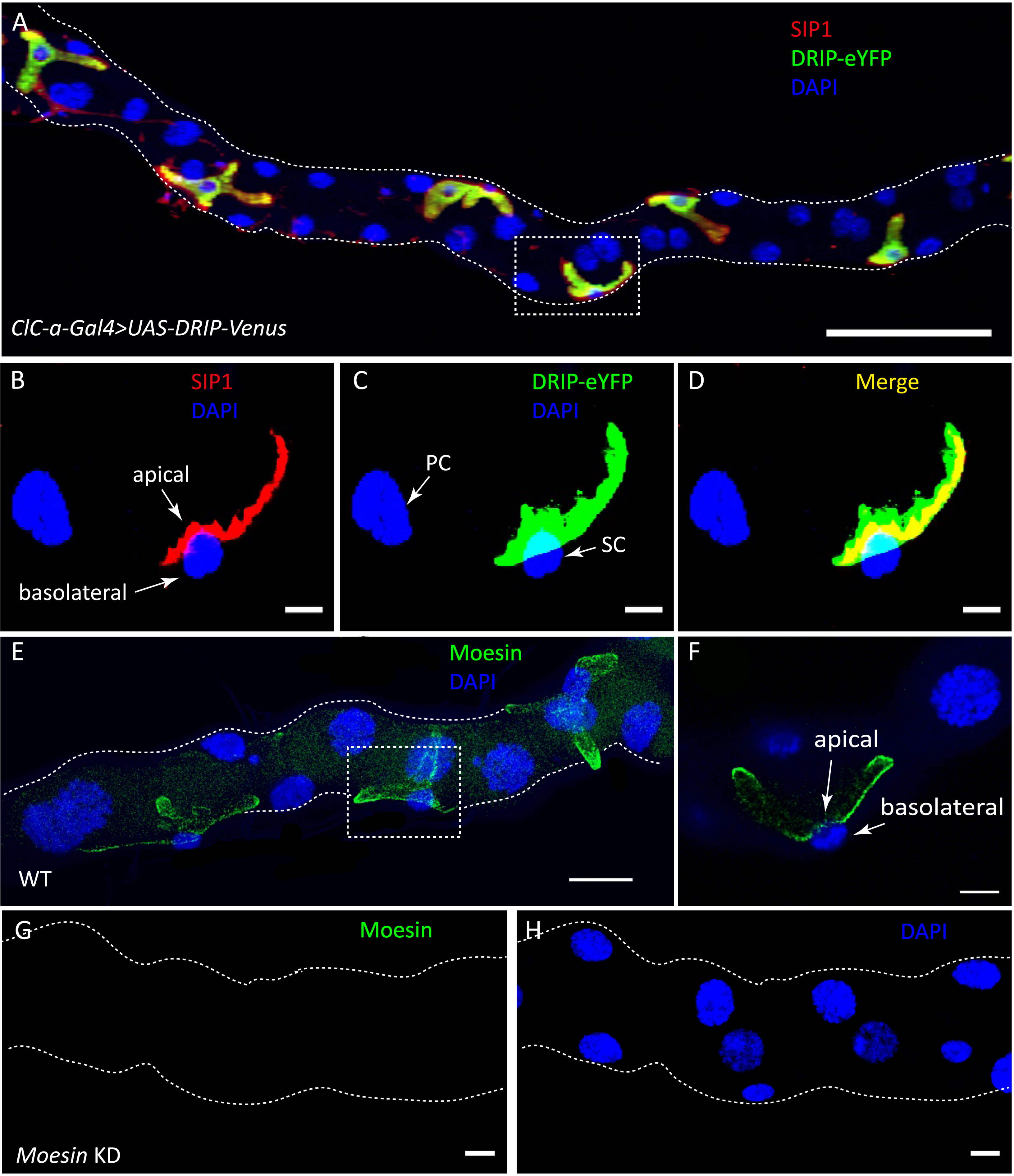
A
SIP1
DRIP-eYFP
DAPI
ClC-a-Gal4>UAS-DRIP-Venus
B
SIP1
DAPI
apical
basolateral
C
DRIP-eYFP
DAPI
PC
SC
D
Merge
E
Moesin
DAPI
WT
F
apical
basolateral
G
Moesin
Moesin KD
H
DAPI

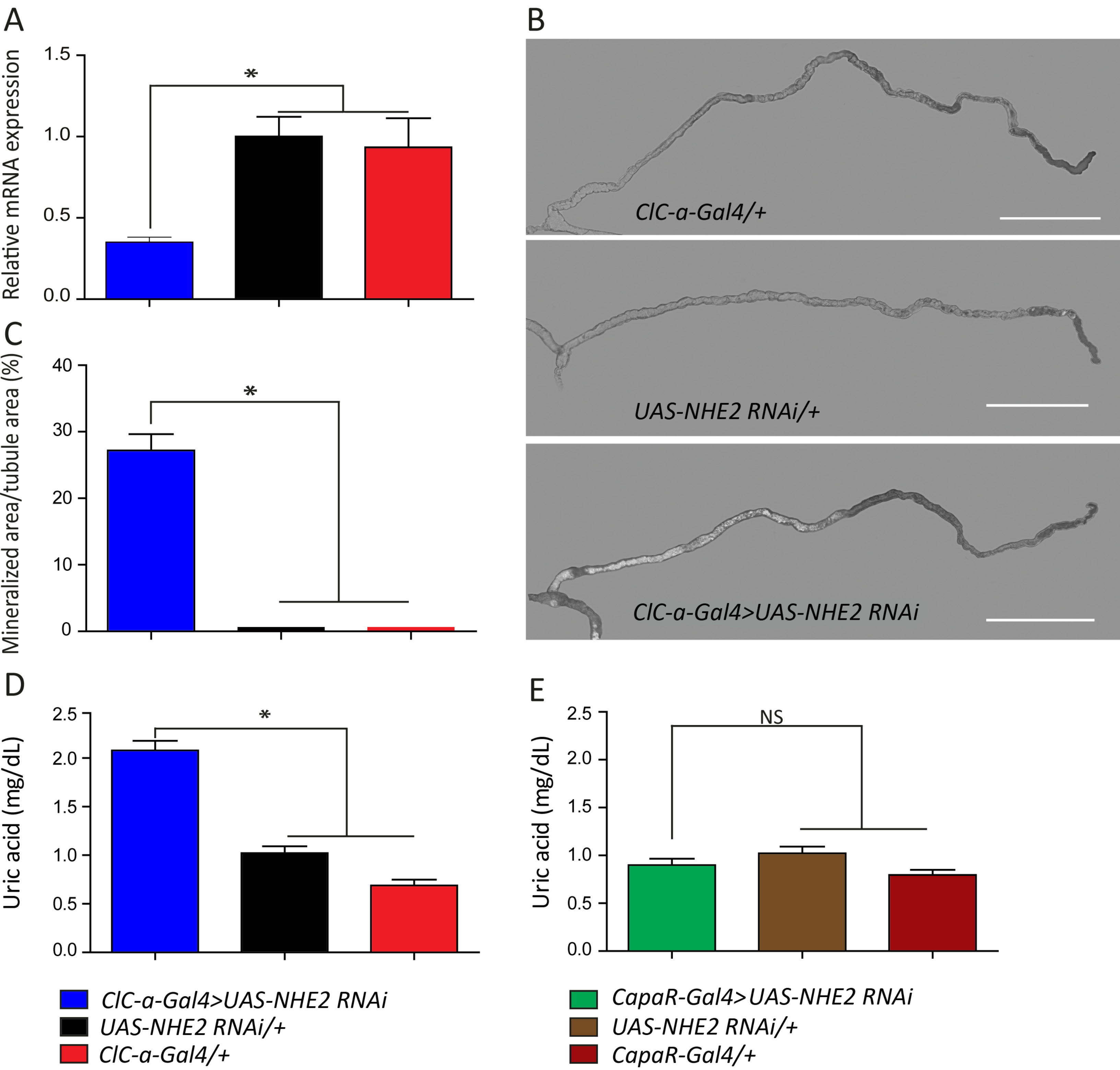

A
Relative mRNA expression
1.5
1.0
0.5
0.0
*
B
ClC-a-Gal4/+
UAS-NHE2 RNAi/+
ClC-a-Gal4>UAS-NHE2 RNAi
C
Mineralized area/tubule area (%)
40
30
20
10
0
*
D
Uric acid (mg/dL)
2.5
2.0
1.5
1.0
0.5
0.0
*
E
Uric acid (mg/dL)
2.5
2.0
1.5
1.0
0.5
0.0
NS
ClC-a-Gal4>UAS-NHE2 RNAi
UAS-NHE2 RNAi/+
ClC-a-Gal4/+
CapaR-Gal4>UAS-NHE2 RNAi
UAS-NHE2 RNAi/+
CapaR-Gal4/+

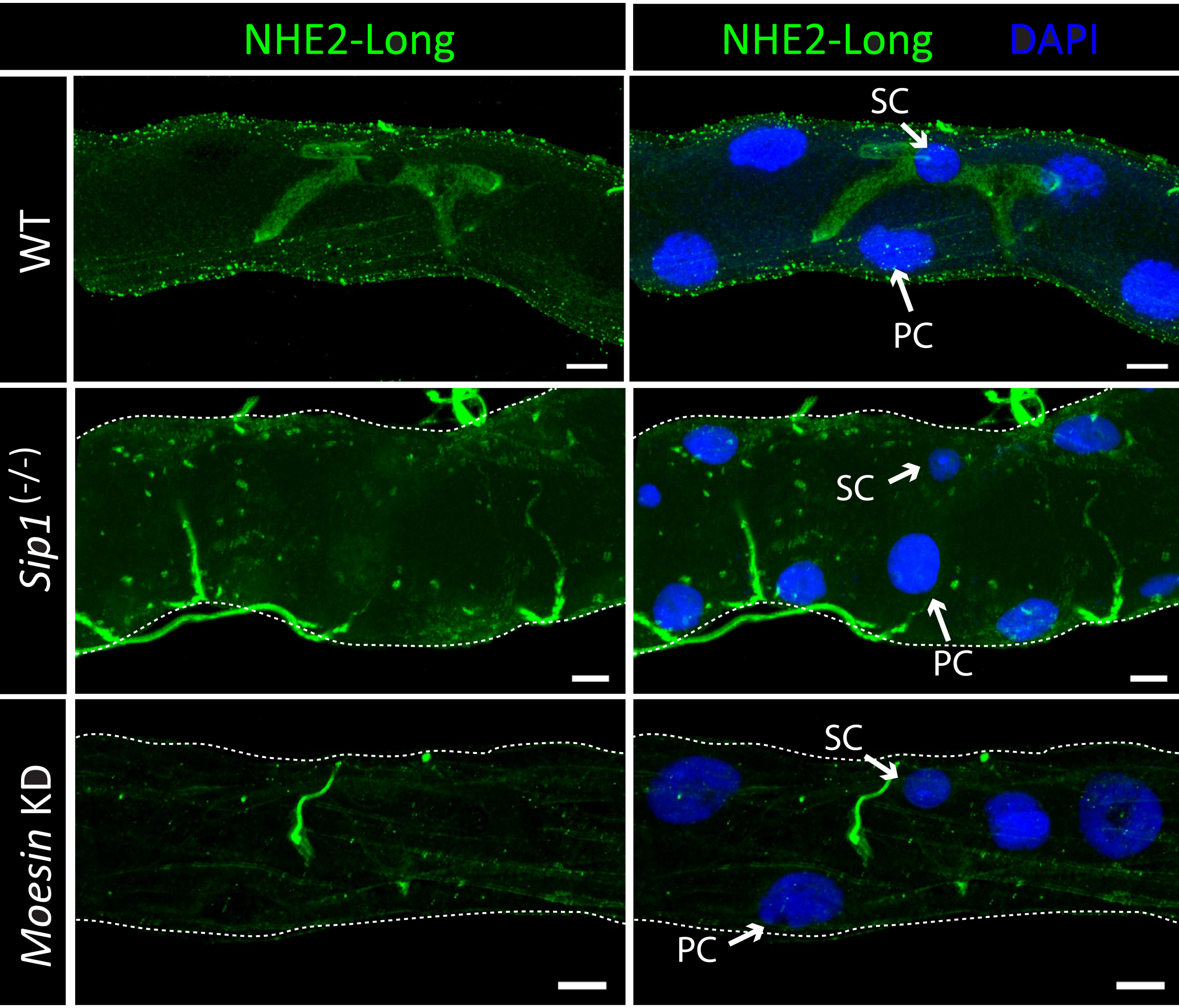

NHE2-Long
NHE2-Long DAPI
WT
Sip1 (-/-)
Moesin KD
SC
PC
SC
PC
SC
PC

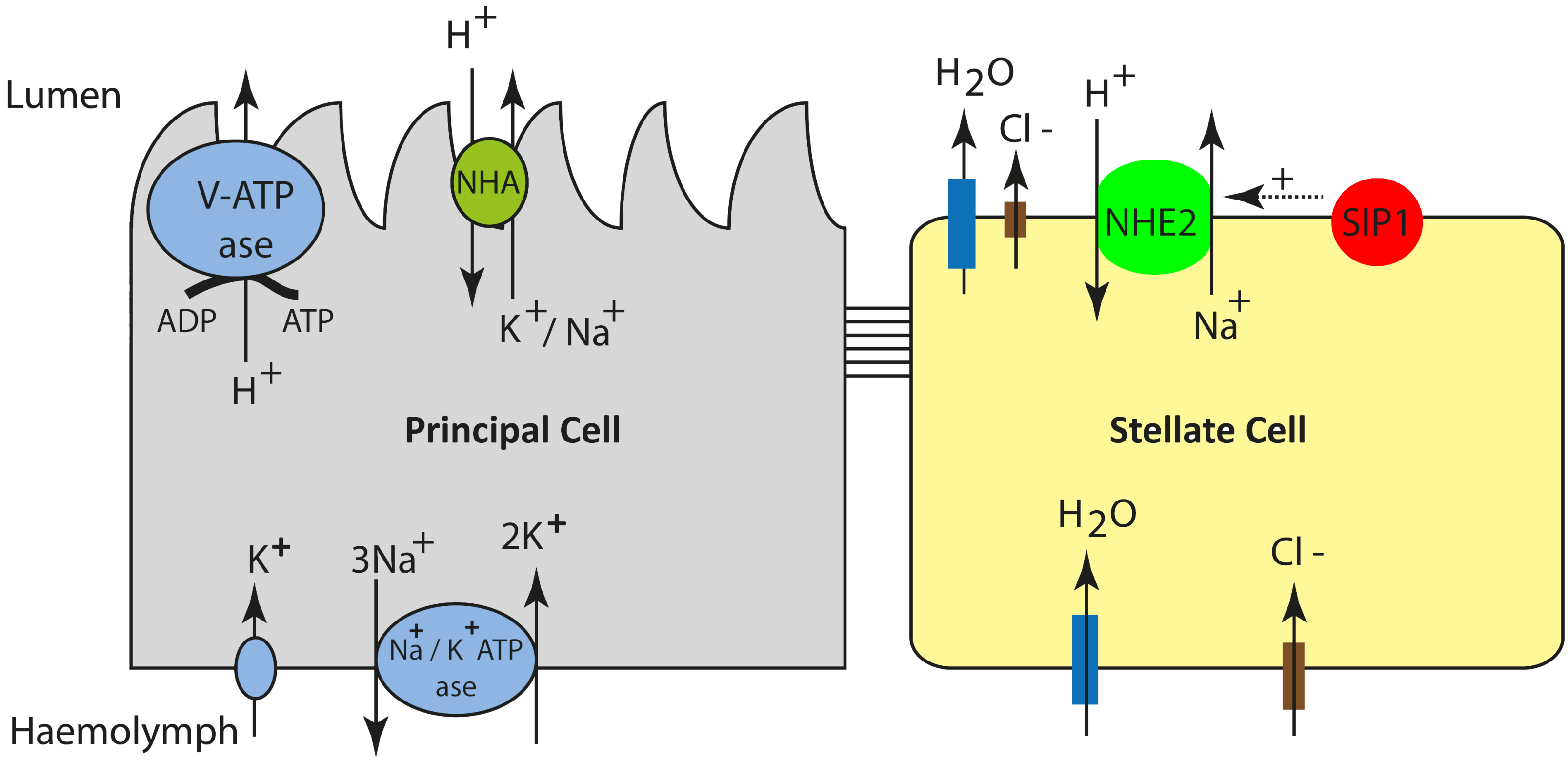
Lumen
V-ATP
ase
ADP
ATP
H+
H+
NHA
K+/ Na+
H2O
Cl -
H+
NHE2
Na+
+
SIP1
Principal Cell
Stellate Cell
K+
3Na+
2K+
Na+/ K+ ATP
ase
H2O
Cl -
Haemolymph